

Explore In-Context Segmentation via Latent Diffusion Models

Chaoyang Wang¹ Xiangtai Li^{2,3} † Henghui Ding² Lu Qi⁴ Jiangning Zhang⁵
Yunhai Tong¹ Chen Change Loy² Shuicheng Yan³

¹Peking University ²S-Lab, NTU ³Skywork AI ⁴UC, Merced ⁵ZJU
cywang@stu.pku.edu.cn xiangtai94@gmail.com †: Project lead

Project Page: <https://wang-chaoyang.github.io/project/refldmseg>

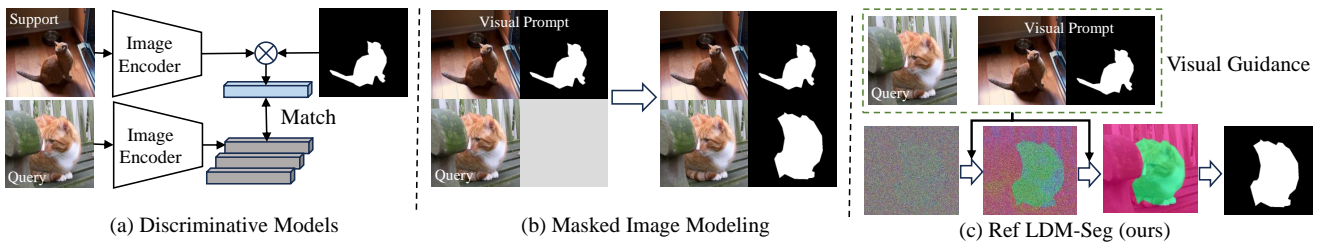


Figure 1. Method comparison. (a) The discriminative models perform query and support prototypes matching. (b) Masked image modeling methods adopt inpainting training. (c) Our LDM-based model generates segmentation masks under the guidance of visual prompts.

Abstract

In-context segmentation has drawn more attention with the introduction of vision foundation models. Most existing approaches adopt metric learning or masked image modeling to build the correlation between visual prompts and input image queries. In this work, we explore this problem from a new perspective, using one representative generation model, the latent diffusion model (LDM). We observe a task gap between generation and segmentation in diffusion models, but LDM is still an effective minimalist for in-context segmentation. In particular, we propose two meta-architectures and correspondingly design several output alignment and optimization strategies. We have conducted comprehensive ablation studies and empirically found that the segmentation quality counts on output alignment and in-context instructions. Moreover, we build a new and fair in-context segmentation benchmark that includes both image and video datasets. Experiments validate the efficiency of our approach, demonstrating comparable or even stronger results than previous specialist models or visual foundation models. Our study shows that LDMs can also achieve good enough results for challenging in-context segmentation tasks.

1. Introduction

In-context learning [4, 6, 10] provides a new perspective for cross-task modeling for vision and NLP. It enables the model to learn and predict according to the prompts. GPT-3 [10] firstly defines in-context learning, which is interpreted as inferring on unseen tasks conditioning on some input-output pairs given as contexts. Several works [6, 17, 82, 83, 86] also explore in-context learning in vision, where the prompts are the visual task input-outputs.

As for the segmentation field, it plays the same role as the few-shot segmentation (FSS) [41, 44, 65, 69]. Most approaches calculate the matching distance between query images and support images (known as visual prompts for in-context learning). To overcome the strict constraints on data volume and category in FSS, and to enable generalization across different tasks, several works [6, 44, 82, 83] recently extend the concept to in-context segmentation and formulate it as a mask generalization task (Fig. 1(b)). This is fundamentally different from those matching or prototype-based discriminative models (Fig. 1(a)) since it directly generates image masks via mask decoding. However, these approaches always need massive datasets to learn such correspondence.

Most recently, latent diffusion models (LDM) [25, 66, 99] demonstrate great potential for generative tasks. Sev-

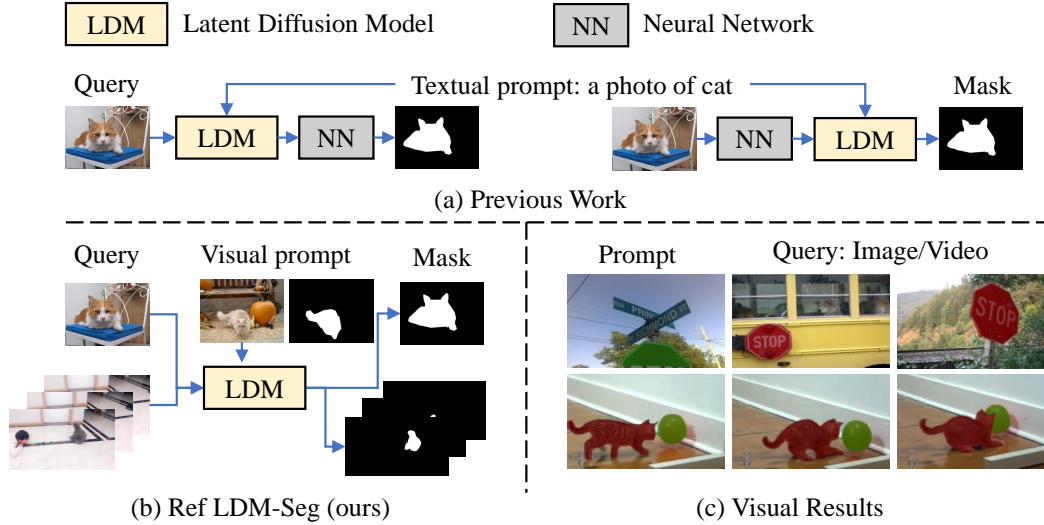


Figure 2. **Latent diffusion model for in-context segmentation.** (a) Previous works mainly rely on textual prompts and additional neural networks for segmentation. (b) Our proposed minimalist framework, Ref LDM-Seg. (c) Segmentation results on images and videos.

eral works [66, 99] show excellent performance in conditional image content creation. Although LDM was initially proposed for generation, there have been some attempts to use it for perceptual tasks. Fig. 2(a) illustrates the mainstream pipeline [7, 19, 90, 103] for LDM-based segmentation. They typically rely on textual prompts for semantic guidance and additional neural networks to assist with LDM. However, the former may not always be available in real-world scenarios, and the latter hinders exploring the LDM’s own segmentation capabilities. Reliance on these auxiliary components might lead to poor model performance in their absence. We design a baseline model, which adopts the LDM as a feature extractor, and test this hypothesis in Sec. 4.4. Moreover, although [77] models the segmentation process without these additional designs, it lacks the capability for in-context segmentation. Motivated by the above analysis, we argue whether in-context segmentation can be formulated as an image mask generation process that can fully explore the generation potential of LDMs.

In this paper, for the first time, we explore the potential of diffusion models for in-context segmentation, as shown in Fig. 1(c). We aim to answer the following novel questions: 1) Whether LDMs can perform in-context segmentation and achieve good enough results? 2) Which meta-architecture in LDM is best suited for in-context segmentation? 3) How do in-context instructions and output alignment affect the LDM’s performance?

To address the questions above, we propose a minimalist LDM-based in-context segmentation framework, Ref LDM-Seg, as shown in Fig. 2(b). Ref LDM-Seg relies on *visual prompts* for guidance *without any subsequent neu-*

ral networks. We analyze three significant factors: instruction extraction, output alignment, and meta-architectures. First, we propose a simple but effective instruction extraction strategy. The experiments show that the instructions obtained in this manner can provide effective guidance, and our model demonstrates robustness to incorrect instructions. Next, to align with the binary segmentation mask and 3-channel image, we design a new output alignment target via pseudo masking modeling. Then, we propose two meta-architectures, namely Ref LDM-Seg-f and Ref LDM-Seg-n. They differ in input formulation, denoising steps, and optimization targets, as shown in Fig. 3. In particular, we design two optimization targets for Ref LDM-Seg-f, respectively, in pixel and latent space. The experiments demonstrate the importance of output alignment. Unlike methods [83], our focus is primarily on the impact of architecture rather than data. As such, we seek to keep a certain amount of training data, which is larger than the few-shot training dataset but much smaller than that of the foundation model. To this end, finally, we propose a size-limited in-context segmentation benchmark consisting of image semantic segmentation, video object segmentation, and video semantic segmentation. We conduct comprehensive ablation studies and broadly compare our method with previous works to demonstrate its effectiveness.

In this paper, we empirically show that:

- *There exists a task gap between generation and segmentation in diffusion models.* However, LDM can still act as an effective minimalist for in-context segmentation.
- *The visual prompts and output alignment both play an essential role in LDM-based in-context segmentation. The success of the segmentation is determined by the former,*

while the latter affects its quality.

- During the denoising process, the LDM-based model outputs low-frequency information first, followed by those with higher frequency.
- Our proposed joint dataset avoids over-fitting and does not compromise the generalization capability to out-of-domain data.

2. Related Work

Diffusion Model. Diffusion models [25, 71, 72] have shown remarkable performance on generation tasks, such as image generation [13, 27, 62, 64, 66, 99], image editing [9, 24, 45, 54, 59, 67, 93], image super resolution [26, 68], video generation [22, 92], and point cloud [56–58, 96, 105]. Although the diffusion model is initially designed for generation tasks, several works employ it for segmentation through two pipelines. The first pipeline treats the diffusion model as a feature extractor. These works [7, 19, 34, 42, 47, 78, 88, 90, 103] typically rely on a decoder head for post-processing. Conversely, the second pipeline [2, 11, 12, 20, 38, 55] extracts features through a pre-trained backbone, then employs the diffusion model as the decoder head. These additional neural networks greatly influence our judgment of the true capabilities of diffusion model *itself* in the segmentation task. Moreover, many of these works require textual prompts for guidance. However, the textual prompts, such as categories or captions, are not always available in real-world scenarios.

In-context Learning. GPT-3 [10] firstly defines in-context learning, which is interpreted as inferring on unseen tasks conditioning on some input-output pairs given as contexts, also known as prompts. As a new concept in computer vision, in-context learning motivates several attempts [1, 4, 6, 52, 80–83, 102]. The work [6] is the first to adopt masked image modeling (MIM) [5, 23, 89] as a visual in-context framework. Painter [82] and SegGPT [83] follow the same spirit but scale up with massive training data. Different from MIM, we aim to explore in-context segmentation with the latent diffusion model to explore the potential of condition generation.

Few-shot Segmentation. Few-shot segmentation aims to segment query images given support samples. The current works [14, 15, 40, 49–51, 75, 79, 91, 104] typically draw on the idea of metric learning by matching spatial location features with semantic centroids. Furthermore, two-branch conditional networks [53, 65, 69], 4D dense convolution [28, 61], data augmentation [74, 76, 101] and transformer-based architecture [35, 70, 87, 98] are also widely adopted by researchers. Although few-shot segmentation and in-context segmentation share a similar episode paradigm, the dataset used in few-shot segmentation is typically very small, making the model prone to overfitting. This may influence the evaluation of the generalization abil-

ity.

Parameter Efficient Tuning. These methods [21, 29, 30, 39, 46, 85, 94, 95] aim to fine-tune only a tiny portion of parameters to adapt the pre-trained foundation models to various downstream tasks. They maintain the pre-trained knowledge of the foundation models. However, they suffer from inadequate expressive power. In our experiments, we adopt the low-rank adaptation (LoRA) [30], a tool widely used in diffusion models, to demonstrate the task gap between generation and segmentation. Although some works [3, 18, 33] try to avoid the dilemma by fine-tuning the prompts only, it is time-costly to learn and restore a new embedding for each prompt. In contrast, we employ a prompt encoder to extract in-context instructions from prompts.

3. Method

In this section, we first revisit the diffusion model, clarify our setting, and provide notations (Sec. 3.1). We then introduce our framework, Ref LDM-Seg, in Sec. 3.2. We discuss three crucial components: instruction extraction, output alignment, and meta-architecture.

3.1. Preliminaries

Diffusion Model. Diffusion models belong to probabilistic generative models that define a chain of forward and backward processes. In the forward process, the model gradually corrupts the data sample z_0 into a noisy latent z_t for $t \in 1..T$: $q(z_t|z_0) = \mathcal{N}(z_t; \sqrt{\bar{\alpha}_t}z_0, (1 - \bar{\alpha}_t)I)$, where $\bar{\alpha}_t = \prod_{s=0}^t \alpha_s = \prod_{s=0}^t (1 - \beta_s)$ and β is the noise schedule. During the training, the model learns to predict the noise $\epsilon_\theta(z_t, t)$ under the supervision of L_2 loss as $\mathcal{L} = \frac{1}{2} \|\epsilon_\theta(z_t, t) - \epsilon(t)\|^2$. During the inference, the model starts from a random noise $z_T \sim \mathcal{N}(0, 1)$, and gradually predicts the noise. Then, it reconstructs the original data z_0 with T steps based on the estimated noise.

Task Setting. We define in-context segmentation (ICS) as a task of combining few-shot segmentation (FSS) and video semantic segmentation (VSS). Our ICS setting **differs** from standard few-shot in the following three aspects:

- **Dataset Size.** Compared with few-shot segmentation, our proposed ICS uses a larger dataset to improve generalization and avoid over-fitting on specific datasets.
- **Data Category.** Realistic scenarios do not strictly distinguish between base classes and novel classes. Our proposed in-context segmentation is more practical.
- **Data Type.** Our proposed in-context segmentation incorporates images and videos into the same framework, which conforms better to the trend of generalist models.

Notation. Fig. 3 illustrates the training process. Our model f takes as inputs two components, namely the in-context instruction τ and the latent variable z_t , and outputs the latent prediction \tilde{z}_t . The detailed composition of z_t is de-

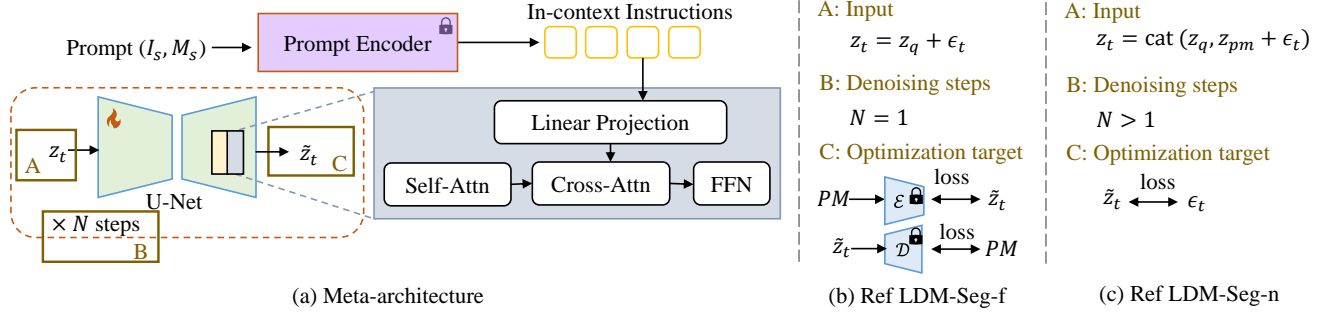


Figure 3. **Our proposed Ref LDM-Seg.** **Left:** Meta-architecture. Our model operates as a minimalist and generates the mask under the guidance of in-context instructions. **Right:** The two variants of our meta-architecture differ in input formulation, denoising time steps, and optimization target. Detailed notations are illustrated in Sec. 3.1.

scribed in Sec. 3.2. t means the time step. The instruction τ is extracted from prompts by prompt encoder E_τ . Each prompt contains one image I_s and the corresponding mask M_s . Moreover, a pair of VAE encoder \mathcal{E} and decoder \mathcal{D} are employed. \mathcal{E} compresses query image I_q into z_q . The model’s output \tilde{z}_t is designed to align with the pseudo mask PM in Ref LDM-Seg-f. In Ref LDM-Seg-n, \tilde{z}_t aligns with the noise ϵ_t .

3.2. Framework

The LDM is initially designed for generative tasks. Most of the work [19, 103] that applies LDM to segmentation requires subsequent neural networks to handle intermediate features or imperfect segmentation results. However, as a generation model, adopting such a design does not realize the generation potential of LDM. To this end, we chose Stable Diffusion as the base model with minimum changes to explore such potential. This subsection explores three key factors influencing the process: instruction extraction, output alignment, and meta-architectures.

Instruction Extraction. Instructions play an important role in LDM. They act as the compressed representation of the prompt, controlling the model to focus on the region of interest and guiding the denoising process. Stable Diffusion encodes textual prompts into instructions using CLIP. To align with pre-trained weights, we use CLIP ViT as our prompt encoder. The instructions are the output of the last hidden layers, except for the first token. We use a linear layer as an adapter to transform the dimension of the instructions. The annotation mask M_s is used as an attention map in cross-attention layers, forcing the model to focus on those tokens that belong to the foreground regions:

$$\tau = E_\tau(I_s), \tau_i = F_i(\tau), \quad (1)$$

where F_i indicates the i^{th} adapter we use and τ_i are the corresponding instructions for i^{th} cross-attention layer.

Output Alignment. It is important to note that we employ LDM for the segmentation task, so the inconsistency

between 1-channel masks and 3-channel images is non-negligible. A pseudo mask must be designed to align the gaps as an intermediate step toward the binary segmentation mask. We argue that a good pseudo mask strategy should meet the following requirements: 1) Binary masks can be obtained from the pseudo masks through simple arithmetic operations. 2) The pseudo masks should be informative beyond binary values.

An intuitive method follows a mapping rule that transforms the binary masks M to 3-channel pseudo masks PM_v :

$$PM_{vi} = \begin{cases} (b, a, (a+b)/2), & M_i \in bg \\ (a, b, (a+b)/2), & M_i \in fg \end{cases} \quad (2)$$

where bg and fg indicate background and foreground, respectively. M_i is the value in position i . a, b are both scalar, indicating the value of a specific channel in the pseudo masks. We set $a < b$.

It is easy to recover the binary segmentation mask with simple arithmetic operations:

$$\tilde{M} = \tilde{PM}_v[1] > \tilde{PM}_v[0]. \quad (3)$$

where \tilde{M} and \tilde{PM}_v indicate the predicted segmentation mask and vanilla pseudo masks, respectively. $[k]$ means the value in the k^{th} channel.

Beyond the vanilla design, we also propose an augmented strategy to fuse the information of images into pseudo masks. Denote the image as I , and the augmented pseudo masks are formulated as follows:

$$PM_{ai} = \begin{cases} (b, a, (a+b)/2) + I_i/\alpha, & M_i \in bg \\ (a, b, (a+b)/2) + I_i/\alpha, & M_i \in fg \end{cases} \quad (4)$$

where α controls the strength of the information of image, and I_i is the value in position i . We set $\alpha > 1$ and $a < b$.

We can obtain the binary segmentation masks \tilde{M} with

simple arithmetic operations:

$$\begin{aligned} PM_a^- &= \tilde{P}M_a - I_i/\alpha, \\ \tilde{M} &= PM_a^-[1] > PM_a^-[0]. \end{aligned} \quad (5)$$

Meta-architectures. As shown in Fig. 3, we explore two representative meta-architectures, namely Ref LDM-Seg-f and Ref LDM-Seg-n. The difference between them mainly lies in the *optimization target* and *denoising time steps*.

Ref LDM-Seg-f indicates **one-step denoising process** and the optimization target is the segmentation mask itself. As shown in Fig. 3(a), a noise variant ϵ_t is added to the latent variant z_q . Our ICS model f , U-Net, takes as input the noisy latent $z_t = z_q + \epsilon_t$, where ϵ_t is the output of the noise scheduler, t controls the noise strength.

We adopt the low-rank adaptation strategy to maintain the knowledge of pre-trained weights and avoid catastrophic forgetting. All parameters are frozen except those q, k, v, o projections in attention layers. We propose two optimization strategies that align the model outputs with the ground truth in the pixel space (6) or in the latent space (7), respectively. We employ the L2 loss, typically used in LDM, rather than any explicit segmentation loss.

$$\mathcal{L}_{fp} = \mathbb{E}_{z_t, \tau} \left[\|PM - \tilde{P}M_t\|_2^2 \right], \quad (6)$$

$$\mathcal{L}_{fl} = \mathbb{E}_{z_t, \tau} \left[\|z_{pm} - \tilde{z}_t\|_2^2 \right], \quad (7)$$

where $\tilde{P}M_t = \mathcal{D}(\tilde{z}_t)$ and $z_{pm} = \mathcal{E}(PM)$.

In the inference stage, Ref LDM-Seg-f conducts only a one time step and outputs the segmentation (pseudo) masks. The video is treated as a sequence of images. The first frame and its annotation are used as prompts, and subsequent frames are inferred conditioned on it. For videos containing multiple categories, we first calculate the probability of each category as a foreground in turn and then select the category with the highest probability:

$$\begin{aligned} \tilde{p}_c &= \frac{\exp(PM[1])}{\exp(PM[0])}, \\ p_c &= \frac{\tilde{p}_c}{1 + \sum_{i=1}^C \tilde{p}_i}, \end{aligned} \quad (8)$$

where \tilde{p}_c indicates the normalized foreground probability map for category c . $PM[i]$ means the value in channel i of pseudo masks. It is obvious that \tilde{p}_0 , as the background’s probability, equals 1.

Ref LDM-Seg-n indicates **multi-step denoising process** and employs an indirect optimization strategy. Unlike Ref LDM-Seg-f, it starts from Gaussian noise and gradually denoises to get the final segmentation mask.

A plain Stable Diffusion architecture is not suitable for Ref LDM-Seg-n. We make minimal but necessary modifications to the architecture by extending the input dimension from 4 to 8. Specifically, denote the latent expression

Table 1. **Details of the combined datasets.** We choose two image semantic segmentation (ISS) datasets, one video object segmentation (VOS) dataset, and one video semantic segmentation (VSS) dataset. (N) means the equivalent number of images.

Dataset	Task	#Category	#Videos		#Images	
			Train	Val	Train	Val
PASCAL [16]	ISS	20	-	-	10582	2000
COCO [48]	ISS	80	-	-	82081	5000
DAVIS-16 [63]	VOS	-	30	16	(2064)	(1023)
VSPW [60]	VSS	58	1000	100	(16473)	(10002)

of query image and pseudo mask as $z_q \in \mathbb{R}^{4 \times H \times W}$ and $z_{pm} \in \mathbb{R}^{4 \times H \times W}$, we get $z_t \in \mathbb{R}^{8 \times H \times W}$ by concatenating the noisy pseudo mask latent with z_q in the channel dimension. The noisy pseudo mask latent is obtained by adding noise ϵ_t to z_{pm} :

$$z_t = \text{concat}((z_{pm} + \epsilon_t); z_q), \quad (9)$$

where the noise scheduler determines t .

Similar to Ref LDM-Seg-f, the ICS model f takes as input the latent variable z_t and the instructions τ , but outputs the estimation of the noise rather than the pseudo mask. We also adopt L2 loss as follows:

$$\mathcal{L}_n = \mathbb{E}_{z_t, t, \tau} \left[\|\epsilon_t - \tilde{z}_t\|_2^2 \right]. \quad (10)$$

To minimize the randomness brought by initial noise, strengthen the guidance of in-context instructions, and maintain the consistency between the outputs and the queries, we adopt classifier-free guidance (CFG) [27]. In the training stage, the query latent z_q and condition τ are randomly set to null embedding with probability $p = 0.05$.

We also adopt CFG in the inference stage. Specifically, Ref LDM-Seg-n outputs the $\tilde{z}_t(z_q, \tau)$ on the basis of three conditional outputs $\tilde{z}_t(z_q, \tau)$, $\tilde{z}_t(\emptyset, \emptyset)$, $\tilde{z}_t(z_q, \emptyset)$ (Equ. 11).

$$\begin{aligned} \tilde{z}_t(z_q, \tau) &= \tilde{z}_t(\emptyset, \emptyset) \\ &\quad + \gamma_q \cdot (\tilde{z}_t(z_q, \emptyset) - \tilde{z}_t(\emptyset, \emptyset)) \\ &\quad + \gamma_\tau \cdot (\tilde{z}_t(z_q, \tau) - \tilde{z}_t(z_q, \emptyset)), \end{aligned} \quad (11)$$

where γ_q and γ_τ control the guidance of query and in-context instruction, respectively.

4. Empirical Study

In this section, we explore the Ref LDM-Seg on in-context segmentation empirically. We first demonstrate the experimental settings in Sec. 4.1. Then, we conduct a comprehensive analysis of how frameworks (Sec. 4.2) and data (Sec. 4.3) influence our model, respectively. Finally, we report the results compared with other methods in Sec. 4.4.

Table 2. **Ablation results on framework.** Models without LoRA mean that all parameters are trainable. PM_a represents the augmented pseudo mask (Equ. 4). PO / LO means pixel space optimization (Equ. 6) / latent space optimization (Equ. 7) respectively.

(a) The effect of meta-architectures and LoRA.			(b) Output alignment of Ref LDM-Seg-n.			(c) Optimization space of Ref LDM-Seg-f.			(d) Rank in Ref LDM-Seg-f.	
Meta-architecture	LoRA	mIoU	LoRA	PM_a	mIoU	LoRA	Optim. Space	mIoU	Rank	mIoU
Ref LDM-Seg-f	-	52.6	✓	-	24.1	-	PO	52.6	1	52.8
	✓	59.6	-	✓	39.3	✓	PO	59.6	4	55.9
Ref LDM-Seg-n	-	39.3	✓	✓	31.9	✓	LO	55.9	8	57.9
	✓	31.9								

4.1. Experimental Setup

Benchmark Details. As mentioned in Sec. 3.1, the in-context segmentation model aims to solve multiple tasks with *one* model, regardless of data type and domain. To this end, we adopt several popular public datasets as part of our benchmark (Tab. 1), including PASCAL [16], COCO [48], DAVIS-16 [63] and VSPW [60]. The training data for VSPW is sampled every four frames for each video. All ‘stuff’ categories are annotated as background. The combined dataset has around 100K images for training. Note that our interest focuses on the model’s performance with limited training data rather than an infinite expansion. The scaling law [32] is not our concern.

Implementation Details. We utilize the Stable Diffusion 1.5 model as the initialization and set the resolution as 256×256 . Our model is jointly trained on the combined dataset for 80K iterations with a batch size of 16. We employ an AdamW optimizer and a linear learning rate scheduler. CLIP ViT/L-14 is adopted as the prompt encoder. We set the CFG coefficient for query and instructions as 1.5 and 7, respectively. By default, the rank of LoRA is equal to 4 in all experiments. We use the VAE of Stable Diffusion 1.5 without any fine-tuning.

Our training follows the spirit of episodic learning. For the image dataset, images with the same semantic labels are considered as a pair of queries and prompts. The video dataset follows the image dataset but additionally requires that the query and prompt come from the same video.

In Sec. 4.2 and Sec. 4.3, our model is trained on the combined dataset but evaluated on the COCO dataset. The results for all datasets are reported in Sec. 4.4.

Evaluation Metrics. We adopt the class mean intersection over union as our evaluation metric in empirical study, which is formulated as $mIoU = \frac{1}{C} \sum_{i=1}^C IoU_i$. C is the number of classes except background. We also report the foreground-background IoU for other image-level tasks in our benchmark following [75]. For video-level tasks, we respectively adopt their evaluation metrics in DAVIS-16 [63] and VSPW [60].

4.2. Study on Framework Design

In this subsection, we investigate the impact of two meta-architectures and the corresponding output alignment and optimization strategies from the architectural perspective.

Meta-architecture. Tab. 2a presents a comparison of meta-architecture. We also consider low-rank adaptation (LoRA). Overall, Ref LDM-Seg-f performs better than Ref LDM-Seg-n. In the best case, the former can achieve a performance of 59.6 mIoU, while the latter can only reach 39.3 mIoU. Interestingly, the two meta-architectures demonstrate distinct characteristics depending on whether LoRA is utilized. When using LoRA, Ref LDM-Seg-f gains around seven mIoU improvement, but the performance of Ref LDM-Seg-n drastically decreases.

Output Alignment. The output of Ref LDM-Seg-n at different time steps is presented in Fig. 4, aligned with the augmented pseudo mask (Equ. 4). Interestingly, the target’s relative position is determined at the beginning of the denoising process. The low-frequency signal is generated first. Then, our model gradually generates high-frequency information like shape or texture as the denoising process proceeds. We quantitatively study the effect of output alignment for Ref LDM-Seg-n in Tab. 2b. The augmented pseudo mask (Equ. 4) significantly outperforms the vanilla one (Equ. 2) and improves the performance from 24.1 mIoU to 31.9 mIoU. As the vanilla pseudo mask (Equ. 2) only has two values (foreground and background), we hypothesize that the trivial strategy reduces the capability of Ref LDM-Seg-n to capture the semantics of the image. In this case, the model may learn some shortcuts.

Optimization Space. In Tab. 2c, we study the effects of optimization space for Ref LDM-Seg-f. Optimization in the pixel space (Equ. 6) benefits the model and brings about 3.7 mIoU improvement. Moreover, LoRA seems more critical for optimization space. Ref LDM-Seg-f drops 3.3 mIoU without LoRA, even though it is optimized in the pixel space. The performance of Ref LDM-Seg-f with different LoRA ranks is reported in Tab. 2d. All these models use latent space optimization. Ref LDM-Seg-f (LO, rank=8) in Tab. 2d achieves a mIoU of 57.9, which is close to Ref LDM-Seg-f (PO, rank=4) in Tab. 2c.

Discussion. Our experiments show that *there exists a task*

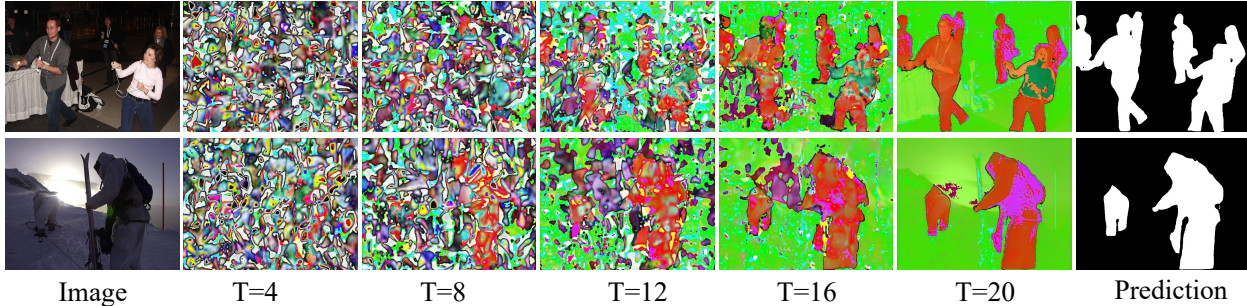


Figure 4. **Visualizations at different time steps.** Ref LDM-Seg-n captures low-frequency information at the beginning of the denoising process and generates high-frequency information as the denoising process approaches completion. The number of denoising steps is 20.

Table 3. **More ablation results for various datasets.**

(a) Effects of combined dataset using Ref LDM-Seg-f.		(b) Performance on FSS1000 dataset.		(c) Ref LDM-Seg-f with multiple instructions.		(d) Effects of pre-trained weight. We explore various LDMs.		
PASCAL COCO		Method	mIoU	Num. of Instructions	mIoU	Meta-architecture	Setting	mIoU
PASCAL (Single)	80.8 39.3	Painter	61.7	1	55.9	Ref LDM-Seg-f	SDXL+512	67.3
COCO (Single)	78.1 56.9	PerSAM	68.5	3	60.8		SD1.5+256	59.6
Combined Dataset (ours)	81.4 55.9	Ref LDM-Seg-f	69.8	5	63.3	Ref LDM-Seg-n	SDXL+512	29.3
				10	63.5		SD1.5+512	26.0
							SD1.5+256	39.3

gap between generation and segmentation for LDM. Intuitively, Ref LDM-Seg-f outputs the segmentation mask directly, aligning with mainstream segmentation models. In contrast, Ref LDM-Seg-n gradually denoises in the latent space. Experiments related to LoRA also support the hypothesis above. LoRA retains most of the pre-trained knowledge while limiting its expressive power, which hinders the performance of Ref LDM-Seg-n.

4.3. Study on Various Datasets

In-context Instruction. Our model segments the target region based on in-context instructions. Fig. 5 illustrates some examples. In the first and second cases, our model accurately segments the target region based on the single instruction provided. The third case shows the model can accept several different instructions without performance degradation. In the fourth case, the provided instruction becomes ineffective when it conflicts with the query.

Tab. 3c reports the results with the number of instructions from 1 to 10. The model’s performance improves as the number of instructions increases, saturating at 63.3 mIoU with five instructions. Further increasing the number of instructions results in only a slight further improvement.

Out-of-domain Dataset. We also test our model on an out-of-domain dataset, FSS1000 [43]. This dataset includes 1000 categories that were not present in the training data. Additionally, it contains numerous ‘stuff’ categories labeled as background during training. We compare with two representative generalist methods, Painter [82] and

PerSAM [100]. Our proposed Ref LDM-Seg-f outperforms these methods and achieves an mIoU of 69.8.

Dataset Combination. Tab. 3a presents the outcomes of Ref LDM-Seg-f trained on a single dataset. The model exhibits overfitting when trained solely on a small dataset like PASCAL. Conversely, the model trained exclusively on the COCO dataset demonstrates superior results on COCO, but it lacks generalization compared to the combined dataset.

Pre-trained Weight. We also try to use SDXL [64] for initialization or use a larger resolution, as shown in Tab. 3d. Surprisingly, the two architectures exhibit different characteristics. A larger model like SDXL or a larger resolution is only beneficial for Ref LDM-Seg-f but unsuitable for Ref LDM-Seg-n. This may be due to the task gap discussed in Sec. 4.2.

4.4. Comparison with Previous Methods

We compare our methods with related works on our benchmark and report the performance under the one-shot segmentation dataset.

Benchmark Results. We compare our method with previous baselines in Tab. 4. Specifically, the specialist models belong to the family of discriminative models. Prompt Diffusion [84] uses a ControlNet [99] architecture. Painter [82] belongs to the family of masked image modeling. It is a visual foundation model trained on massive data. PerSAM [100] employs a strong foundation model, SAM [36], for segmentation. We also design LDM-FE, a specialist baseline that employs an LDM [66] to extract features and

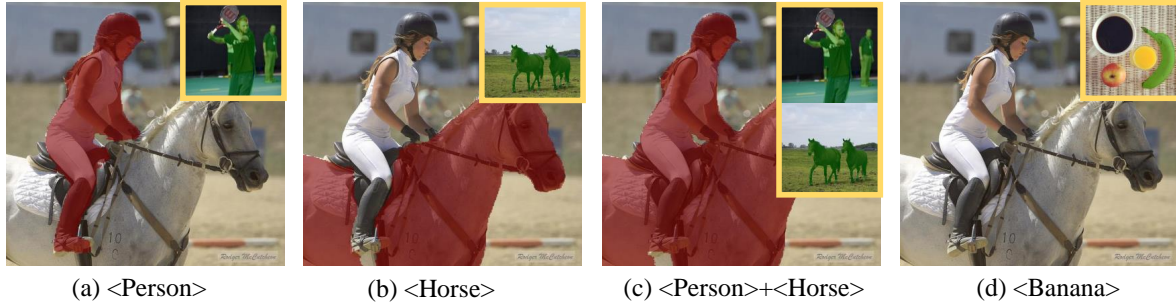


Figure 5. **Combination of instructions.** The output of our model varies based on the instructions located in the top right corner of the query images. (a) and (b) Single instruction. (c) Multiple instructions. (d) Incorrect instruction. Ref LDM-Seg-f is used for the demonstration.

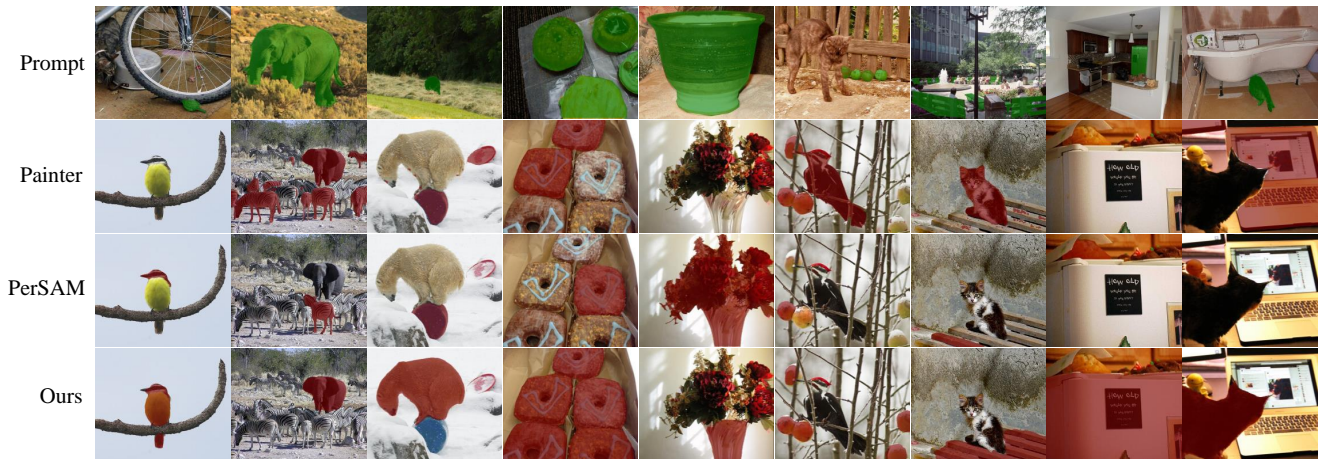


Figure 6. Visualization of segmentation results. We compare our Ref LDM-Seg-f with Painter [82] and PerSAM [100] on COCO dataset.

a PFNet [75] decoder for prediction. In the ICS task, category labels are not available. Therefore, the textual prompt in LDM-FE is set as null.

On image tasks, it can be seen that Ref LDM-Seg-f achieves the best results compared with these methods. Ref LDM-Seg-n also achieves a decent performance of 62.8 mIoU on PASCAL and 39.3 mIoU on COCO. LDM-FE performs similarly to other specialist models but is inferior to Ref LDM-Seg-f, possibly due to the lack of in-context instructions. On video tasks, our models show comparable performance compared with the generalist models. Considering the huge amount of training data used in Painter and SAM, it is acceptable that our method cannot exceed these foundation models on specific metrics.

Fig. 6 shows the visual comparison between our model and previous works on the COCO dataset. It is evident from these results that our model successfully segments the target region, whereas other methods fail to establish the semantic connection between prompt and query, leading to missing and false-positive predictions. Fig. 7 presents more visualizations on video semantic segmentation of the VSPW dataset. From these visual results, our model exhibits ro-

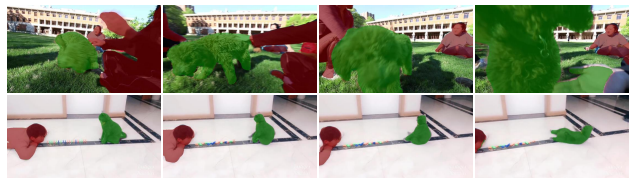


Figure 7. Qualitative results of Ref LDM-Seg-f on VSPW dataset.

bustness to various scenes and categories in both image and video segmentation tasks.

Results on One-shot Segmentation. We also test our model under the few-shot segmentation setting. As shown in Tab. 5, our model achieves decent or better performance on almost all folds of COCO-20ⁱ dataset. Specifically, it significantly outperforms some recently proposed generalist model, PerSAM [100] by around 30% mIoU.

5. Conclusion

For the first time, we explore in-context segmentation via latent diffusion models. We propose two meta-architectures

Table 4. **Benchmark results.** We compare our method with several representative specialist models and generalist models. The **bold** and underlined entries represent the best and second-best performance.

Method	PASCAL		COCO		DAVIS-16			VSPW	
	mIoU	FB-IoU	mIoU	FB-IoU	$\mathcal{J}\&\mathcal{F}$	\mathcal{J}	\mathcal{F}	mIoU	fwIoU
Specialist Models									
PFENet [75]	<u>76.0</u>	87.3	43.2	74.2	-	-	-	-	-
SVF [73]	75.9	87.3	43.8	74.6	-	-	-	-	-
VTM [35]	73.5	84.7	<u>45.4</u>	73.7	-	-	-	-	-
DCAMA [70]	70.7	84.5	37.6	71.0	-	-	-	-	-
CyCTR [97]	75.7	<u>87.4</u>	44.3	<u>74.8</u>	-	-	-	-	-
LDM [66] - FE [75]	72.8	85.3	44.1	73.2	-	-	-	-	-
Generalist Models									
Prompt Diffusion [84]	9.0	40.1	5.9	40.7	-	-	-	-	-
Painter [82]	53.7	69.7	30.8	58.3	76.7	77.9	75.6	12.2	76.7
PerSAM [100]	47.6	69.4	25.5	57.5	68.7	67.7	69.6	42.6	79.1
Diffusion Based Generalist Models									
Ref LDM-Seg-n (ours)	62.8	77.2	39.3	66.1	67.6	67.1	68.1	17.6	71.5
Ref LDM-Seg-f (ours)	83.4	92.0	59.6	82.7	<u>72.4</u>	<u>74.5</u>	<u>70.3</u>	<u>40.5</u>	88.2

Table 5. Results of 1-shot segmentation on COCO-20ⁱ using mIoU metric.

Method	Fold-0	Fold-1	Fold-2	Fold-3	Mean
RePRI [8]	32.0	38.7	32.7	33.1	34.1
HSNet [61]	37.2	44.1	42.4	41.3	41.3
BAM [37]	43.4	50.6	47.5	43.4	46.2
FPTrans [98]	44.4	48.9	50.6	44.0	47.0
MSANet [31]	47.8	57.4	48.7	50.5	51.1
PerSAM [100]	21.8	24.1	20.8	22.6	22.3
Ref LDM-Seg-f (ours)	51.9	58.9	50.0	52.1	53.2

and design several output alignment strategies and optimization methods. We observe a task gap between generation and segmentation in diffusion models, but the LDM itself can be an effective minimalist for in-context segmentation tasks. We also propose an in-context segmentation benchmark and achieve comparable or even better results than specialists or vision foundation models.

Broader Impact. Our work makes a first-step exploration of conditional mask generation for in-context segmentation. Our proposed method provides a unified and general framework. We hope our exploration will attract the community’s attention to the unification of visual generation and perception tasks via diffusion models.

Acknowledgement. This work is supported by the National Key Research and Development Program of China (No. 2023YFC3807600).

References

[1] Jean-Baptiste Alayrac, Jeff Donahue, Pauline Luc, Antoine Miech, Iain Barr, Yana Hasson, Karel Lenc, Arthur

Mensch, Katherine Millican, Malcolm Reynolds, et al. Flamingo: a visual language model for few-shot learning. In *NeurIPS*, 2022. 3

[2] Tomer Amit, Tal Shaharbany, Eliya Nachmani, and Lior Wolf. Segdiff: Image segmentation with diffusion probabilistic models. *arXiv preprint arXiv:2112.00390*, 2021. 3

[3] Hyojin Bahng, Ali Jahanian, Swami Sankaranarayanan, and Phillip Isola. Exploring visual prompts for adapting large-scale models. *arXiv preprint arXiv:2203.17274*, 2022. 3

[4] Ivana Balažević, David Steiner, Nikhil Parthasarathy, Relja Arandjelović, and Olivier J Hénaff. Towards in-context scene understanding. In *NeurIPS*, 2023. 1, 3

[5] Hangbo Bao, Li Dong, Songhao Piao, and Furu Wei. Beit: Bert pre-training of image transformers. In *ICLR*, 2022. 3

[6] Amir Bar, Yossi Gandelsman, Trevor Darrell, Amir Globerson, and Alexei Efros. Visual prompting via image inpainting. In *NeurIPS*, 2022. 1, 3

[7] Dmitry Baranchuk, Ivan Rubachev, Andrey Voynov, Valentin Khruikov, and Artem Babenko. Label-efficient semantic segmentation with diffusion models. In *ICLR*, 2022. 2, 3

[8] Malik Boudiaf, Hoel Kervadec, Ziko Imtiaz Masud, Pablo Piantanida, Ismail Ben Ayed, and Jose Dolz. Few-shot segmentation without meta-learning: A good transductive inference is all you need? In *CVPR*, 2021. 9

[9] Tim Brooks, Aleksander Holynski, and Alexei A Efros. Instructpix2pix: Learning to follow image editing instructions. In *CVPR*, 2023. 3

[10] Tom Brown, Benjamin Mann, Nick Ryder, Melanie Subbiah, Jared D Kaplan, Prafulla Dhariwal, Arvind Neelakantan, Pranav Shyam, Girish Sastry, Amanda Askell, et al. Language models are few-shot learners. In *NeurIPS*, 2020. 1, 3

[11] Shoufa Chen, Peize Sun, Yibing Song, and Ping Luo. Diffusiondet: Diffusion model for object detection. In *ICCV*, 2023. 3

- [12] Ting Chen, Lala Li, Saurabh Saxena, Geoffrey Hinton, and David J Fleet. A generalist framework for panoptic segmentation of images and videos. In *ICCV*, 2023. 3
- [13] Prafulla Dhariwal and Alexander Nichol. Diffusion models beat gans on image synthesis. In *NeurIPS*, 2021. 3
- [14] Henghui Ding, Chang Liu, Shuting He, Xudong Jiang, and Chen Change Loy. MeViS: A large-scale benchmark for video segmentation with motion expressions. In *ICCV*, 2023. 3
- [15] Henghui Ding, Chang Liu, Shuting He, Xudong Jiang, Philip HS Torr, and Song Bai. MOSE: A new dataset for video object segmentation in complex scenes. In *ICCV*, 2023. 3
- [16] Mark Everingham, Luc Van Gool, Christopher KI Williams, John Winn, and Andrew Zisserman. The pascal visual object classes (voc) challenge. *IJCV*, 2010. 5, 6
- [17] Zhongbin Fang, Xiangtai Li, Xia Li, Joachim M Buhmann, Chen Change Loy, and Mengyuan Liu. Explore in-context learning for 3d point cloud understanding. In *NeurIPS*, 2023. 1
- [18] Rinon Gal, Yuval Alaluf, Yuval Atzmon, Or Patashnik, Amit H Bermano, Gal Chechik, and Daniel Cohen-Or. An image is worth one word: Personalizing text-to-image generation using textual inversion. *arXiv preprint arXiv:2208.01618*, 2022. 3
- [19] Zigang Geng, Binxin Yang, Tiankai Hang, Chen Li, Shuyang Gu, Ting Zhang, Jianmin Bao, Zheng Zhang, Han Hu, Dong Chen, et al. Instructdiffusion: A generalist modeling interface for vision tasks. *arXiv preprint arXiv:2309.03895*, 2023. 2, 3, 4
- [20] Zhangxuan Gu, Haoxing Chen, Zhuoer Xu, Jun Lan, Changhua Meng, and Weiqiang Wang. Diffusioninst: Diffusion model for instance segmentation. In *ICASSP*, 2024. 3
- [21] Demi Guo, Alexander M Rush, and Yoon Kim. Parameter-efficient transfer learning with diff pruning. In *ACL*, 2021. 3
- [22] William Harvey, Saeid Naderiparizi, Vaden Masrani, Christian Weillbach, and Frank Wood. Flexible diffusion modeling of long videos. In *NeurIPS*, 2022. 3
- [23] Kaiming He, Xinlei Chen, Saining Xie, Yanghao Li, Piotr Dollár, and Ross Girshick. Masked autoencoders are scalable vision learners. In *CVPR*, 2022. 3
- [24] Amir Hertz, Ron Mokady, Jay Tenenbaum, Kfir Aberman, Yael Pritch, and Daniel Cohen-Or. Prompt-to-prompt image editing with cross attention control. In *ICLR*, 2023. 3
- [25] Jonathan Ho, Ajay Jain, and Pieter Abbeel. Denoising diffusion probabilistic models. In *NeurIPS*, 2020. 1, 3
- [26] Jonathan Ho, Chitwan Saharia, William Chan, David J Fleet, Mohammad Norouzi, and Tim Salimans. Cascaded diffusion models for high fidelity image generation. *The Journal of Machine Learning Research*, 2022. 3
- [27] Jonathan Ho and Tim Salimans. Classifier-free diffusion guidance. In *NeurIPS Workshops*, 2021. 3, 5
- [28] Sunghwan Hong, Seokju Cho, Jisu Nam, Stephen Lin, and Seungryong Kim. Cost aggregation with 4d convolutional swin transformer for few-shot segmentation. In *ECCV*, 2022. 3
- [29] Neil Houlsby, Andrei Giurgiu, Stanislaw Jastrzebski, Bruna Morrone, Quentin De Laroussilhe, Andrea Gesmundo, Mona Attariyan, and Sylvain Gelly. Parameter-efficient transfer learning for nlp. In *ICML*, 2019. 3
- [30] Edward J Hu, Yelong Shen, Phillip Wallis, Zeyuan Allen-Zhu, Yuanzhi Li, Shean Wang, Lu Wang, and Weizhu Chen. Lora: Low-rank adaptation of large language models. In *ICLR*, 2022. 3
- [31] Ehtesham Iqbal, Sirojbek Safarov, and Seongdeok Bang. Msanet: Multi-similarity and attention guidance for boosting few-shot segmentation. *arXiv preprint arXiv:2206.09667*, 2022. 9
- [32] Jared Kaplan, Sam McCandlish, Tom Henighan, Tom B Brown, Benjamin Chess, Rewon Child, Scott Gray, Alec Radford, Jeffrey Wu, and Dario Amodei. Scaling laws for neural language models. *arXiv preprint arXiv:2001.08361*, 2020. 6
- [33] Aliasghar Khani, Saeid Asgari Taghanaki, Aditya Sanghi, Ali Mahdavi Amiri, and Ghassan Hamarneh. Slime: Segment like me. *arXiv preprint arXiv:2309.03179*, 2023. 3
- [34] Bardia Khosravi, Pouria Rouzrokh, John P Mickle, Shahriar Faghani, Kellen Mulford, Linjun Yang, A Noelle Larson, Benjamin M Howe, Bradley J Erickson, Michael J Taunton, et al. Few-shot biomedical image segmentation using diffusion models: Beyond image generation. *Computer Methods and Programs in Biomedicine*, 2023. 3
- [35] Donggyun Kim, Jinwoo Kim, Seongwoong Cho, Chong Luo, and Seunghoon Hong. Universal few-shot learning of dense prediction tasks with visual token matching. In *ICLR*, 2023. 3, 9
- [36] Alexander Kirillov, Eric Mintun, Nikhila Ravi, Hanzi Mao, Chloe Rolland, Laura Gustafson, Tete Xiao, Spencer Whitehead, Alexander C Berg, Wan-Yen Lo, et al. Segment anything. In *ICCV*, 2023. 7
- [37] Chunbo Lang, Gong Cheng, Binfei Tu, and Junwei Han. Learning what not to segment: A new perspective on few-shot segmentation. In *CVPR*, 2022. 9
- [38] Minh-Quan Le, Tam V Nguyen, Trung-Nghia Le, Thanh-Toan Do, Minh N Do, and Minh-Triet Tran. Maskdiff: Modeling mask distribution with diffusion probabilistic model for few-shot instance segmentation. *arXiv preprint arXiv:2303.05105*, 2023. 3
- [39] Brian Lester, Rami Al-Rfou, and Noah Constant. The power of scale for parameter-efficient prompt tuning. In *EMNLP*, 2021. 3
- [40] Gen Li, Varun Jampani, Laura Sevilla-Lara, Deqing Sun, Jonghyun Kim, and Joongkyu Kim. Adaptive prototype learning and allocation for few-shot segmentation. In *CVPR*, 2021. 3
- [41] Xiangtai Li, Henghui Ding, Wenwei Zhang, Haobo Yuan, Guangliang Cheng, Pang Jiangmiao, Kai Chen, Ziwei Liu, and Chen Change Loy. Transformer-based visual segmentation: A survey. *arXiv pre-print*, 2023. 1
- [42] Xinghui Li, Jingyi Lu, Kai Han, and Victor Prisacariu. Sd4match: Learning to prompt stable diffusion model for semantic matching. *arXiv preprint arXiv:2310.17569*, 2023. 3
- [43] Xiang Li, Tianhan Wei, Yau Pun Chen, Yu-Wing Tai, and Chi-Keung Tang. Fss-1000: A 1000-class dataset for few-

- shot segmentation. In *CVPR*, 2020. 7
- [44] Xiangtai Li, Haobo Yuan, Wei Li, Henghui Ding, Size Wu, Wenwei Zhang, Yining Li, Kai Chen, and Chen Change Loy. Omg-seg: Is one model good enough for all segmentation? In *CVPR*, 2024. 1
- [45] Xiangtai Li, Wenwei Zhang, Jiangmiao Pang, Kai Chen, Guangliang Cheng, Yunhai Tong, and Chen Change Loy. Video k-net: A simple, strong, and unified baseline for video segmentation. In *CVPR*, 2022. 3
- [46] Xiang Lisa Li and Percy Liang. Prefix-tuning: Optimizing continuous prompts for generation. In *ACL*, 2021. 3
- [47] Ziyi Li, Qinye Zhou, Xiaoyun Zhang, Ya Zhang, Yanfeng Wang, and Weidi Xie. Open-vocabulary object segmentation with diffusion models. In *ICCV*, 2023. 3
- [48] Tsung-Yi Lin, Michael Maire, Serge Belongie, James Hays, Pietro Perona, Deva Ramanan, Piotr Dollár, and C Lawrence Zitnick. Microsoft coco: Common objects in context. In *ECCV*, 2014. 5, 6
- [49] Jie Liu, Yanqi Bao, Guo-Sen Xie, Huan Xiong, Jan-Jakob Sonke, and Efstratios Gavves. Dynamic prototype convolution network for few-shot semantic segmentation. In *CVPR*, 2022. 3
- [50] Yuanwei Liu, Nian Liu, Qinglong Cao, Xiwen Yao, Junwei Han, and Ling Shao. Learning non-target knowledge for few-shot semantic segmentation. In *CVPR*, 2022.
- [51] Yuanwei Liu, Nian Liu, Xiwen Yao, and Junwei Han. Intermediate prototype mining transformer for few-shot semantic segmentation. In *NeurIPS*, 2022. 3
- [52] Jiasen Lu, Christopher Clark, Rowan Zellers, Roozbeh Mottaghi, and Aniruddha Kembhavi. Unified-io: A unified model for vision, language, and multi-modal tasks. In *ICLR*, 2023. 3
- [53] Zhihe Lu, Sen He, Xiatian Zhu, Li Zhang, Yi-Zhe Song, and Tao Xiang. Simpler is better: Few-shot semantic segmentation with classifier weight transformer. In *ICCV*, 2021. 3
- [54] Andreas Lugmayr, Martin Danelljan, Andres Romero, Fisher Yu, Radu Timofte, and Luc Van Gool. Repaint: Inpainting using denoising diffusion probabilistic models. In *CVPR*, 2022. 3
- [55] Run Luo, Zikai Song, Lintao Ma, Jinlin Wei, Wei Yang, and Min Yang. Diffusiontrack: Diffusion model for multi-object tracking. In *AAAI*, 2024. 3
- [56] Shitong Luo and Wei Hu. Diffusion probabilistic models for 3d point cloud generation. In *CVPR*, 2021. 3
- [57] Shitong Luo and Wei Hu. Score-based point cloud denoising. In *ICCV*, 2021.
- [58] Zhaoyang Lyu, Zhifeng Kong, Xudong Xu, Liang Pan, and Dahua Lin. A conditional point diffusion-refinement paradigm for 3d point cloud completion. In *ICLR*, 2022. 3
- [59] Chenlin Meng, Yutong He, Yang Song, Jiaming Song, Jiajun Wu, Jun-Yan Zhu, and Stefano Ermon. Sdedit: Guided image synthesis and editing with stochastic differential equations. In *ICLR*, 2022. 3
- [60] Jiaxu Miao, Yunchao Wei, Yu Wu, Chen Liang, Guangrui Li, and Yi Yang. Vspw: A large-scale dataset for video scene parsing in the wild. In *CVPR*, 2021. 5, 6
- [61] Juhong Min, Dahyun Kang, and Minsu Cho. Hypercorrelation squeeze for few-shot segmentation. In *ICCV*, 2021. 3, 9
- [62] William Peebles and Saining Xie. Scalable diffusion models with transformers. In *ICCV*, 2023. 3
- [63] Federico Perazzi, Jordi Pont-Tuset, Brian McWilliams, Luc Van Gool, Markus Gross, and Alexander Sorkine-Hornung. A benchmark dataset and evaluation methodology for video object segmentation. In *CVPR*, 2016. 5, 6
- [64] Dustin Podell, Zion English, Kyle Lacey, Andreas Blattmann, Tim Dockhorn, Jonas Müller, Joe Penna, and Robin Rombach. Sdxl: Improving latent diffusion models for high-resolution image synthesis. In *ICLR*, 2024. 3, 7, 13
- [65] Kate Rakelly, Evan Shelhamer, Trevor Darrell, Alexei A. Efros, and Sergey Levine. Conditional networks for few-shot semantic segmentation. In *ICLR*, 2018. 1, 3
- [66] Robin Rombach, Andreas Blattmann, Dominik Lorenz, Patrick Esser, and Björn Ommer. High-resolution image synthesis with latent diffusion models. In *CVPR*, 2022. 1, 2, 3, 7, 9, 13
- [67] Chitwan Saharia, William Chan, Huiwen Chang, Chris Lee, Jonathan Ho, Tim Salimans, David Fleet, and Mohammad Norouzi. Palette: Image-to-image diffusion models. In *SIGGRAPH*, 2022. 3
- [68] Chitwan Saharia, Jonathan Ho, William Chan, Tim Salimans, David J Fleet, and Mohammad Norouzi. Image super-resolution via iterative refinement. *TPAMI*, 2022. 3
- [69] Amirreza Shaban, Shray Bansal, Zhen Liu, Irfan Essa, and Byron Boots. One-shot learning for semantic segmentation. In *BMVC*, 2017. 1, 3
- [70] Xinyu Shi, Dong Wei, Yu Zhang, Donghuan Lu, Munan Ning, Jiashun Chen, Kai Ma, and Yefeng Zheng. Dense cross-query-and-support attention weighted mask aggregation for few-shot segmentation. In *ECCV*, 2022. 3, 9
- [71] Jiaming Song, Chenlin Meng, and Stefano Ermon. Denoising diffusion implicit models. In *ICLR*, 2021. 3
- [72] Yang Song, Jascha Sohl-Dickstein, Diederik P Kingma, Abhishek Kumar, Stefano Ermon, and Ben Poole. Score-based generative modeling through stochastic differential equations. In *ICLR*, 2021. 3
- [73] Yanpeng Sun, Qiang Chen, Xiangyu He, Jian Wang, Haocheng Feng, Junyu Han, Errui Ding, Jian Cheng, Zechao Li, and Jingdong Wang. Singular value fine-tuning: Few-shot segmentation requires few-parameters fine-tuning. In *NeurIPS*, 2022. 9
- [74] Weimin Tan, Siyuan Chen, and Bo Yan. Diffss: Diffusion model for few-shot semantic segmentation. *arXiv preprint arXiv:2307.00773*, 2023. 3
- [75] Zhuotao Tian, Hengshuang Zhao, Michelle Shu, Zhicheng Yang, Ruiyu Li, and Jiaya Jia. Prior guided feature enrichment network for few-shot segmentation. *TPAMI*, 2020. 3, 6, 8, 9
- [76] Nontawat Tritrong, Pitchaporn Rewatbowornwong, and Supasorn Suwajanakorn. Repurposing gans for one-shot semantic part segmentation. In *CVPR*, 2021. 3
- [77] Wouter Van Gansbeke and Bert De Brabandere. A simple latent diffusion approach for panoptic segmentation and mask inpainting. *arXiv preprint arXiv:2401.10227*, 2024. 2
- [78] Qiang Wan, Zilong Huang, Bingyi Kang, Jiashi Feng, and Li Zhang. Harnessing diffusion models for visual percep-

- tion with meta prompts. *arXiv preprint arXiv:2312.14733*, 2023. 3
- [79] Kaixin Wang, Jun Hao Liew, Yingtian Zou, Daquan Zhou, and Jiashi Feng. Panet: Few-shot image semantic segmentation with prototype alignment. In *ICCV*, 2019. 3
- [80] Peng Wang, An Yang, Rui Men, Junyang Lin, Shuai Bai, Zhikang Li, Jianxin Ma, Chang Zhou, Jingren Zhou, and Hongxia Yang. Ofa: Unifying architectures, tasks, and modalities through a simple sequence-to-sequence learning framework. In *ICML*, 2022. 3
- [81] Xinshun Wang, Zhongbin Fang, Xia Li, Xiangtai Li, Chen Chen, and Mengyuan Liu. Skeleton-in-context: Unified skeleton sequence modeling with in-context learning. *arXiv preprint arXiv:2312.03703*, 2023.
- [82] Xinlong Wang, Wen Wang, Yue Cao, Chunhua Shen, and Tiejun Huang. Images speak in images: A generalist painter for in-context visual learning. In *CVPR*, 2023. 1, 3, 7, 8, 9
- [83] Xinlong Wang, Xiaosong Zhang, Yue Cao, Wen Wang, Chunhua Shen, and Tiejun Huang. Seggpt: Segmenting everything in context. In *ICCV*, 2023. 1, 2, 3, 13
- [84] Zhendong Wang, Yifan Jiang, Yadong Lu, Yelong Shen, Pengcheng He, Weizhu Chen, Zhangyang Wang, and Mingyuan Zhou. In-context learning unlocked for diffusion models. In *NeurIPS*, 2023. 7, 9
- [85] Jianzong Wu, Xiangtai Li, Chenyang Si, Shangchen Zhou, Jingkang Yang, Jiangning Zhang, Yining Li, Kai Chen, Yunhai Tong, Ziwei Liu, et al. Towards language-driven video inpainting via multimodal large language models. *CVPR*, 2024. 3
- [86] Jianzong Wu, Xiangtai Li, Shilin Xu, Haobo Yuan, Henghui Ding, Yibo Yang, Xia Li, Jiangning Zhang, Yunhai Tong, Xudong Jiang, Bernard Ghanem, and Dacheng Tao. Towards open vocabulary learning: A survey. *T-PAMI*, 2024. 1
- [87] Guo-Sen Xie, Huan Xiong, Jie Liu, Yazhou Yao, and Ling Shao. Few-shot semantic segmentation with cyclic memory network. In *ICCV*, 2021. 3
- [88] Jiahao Xie, Wei Li, Xiangtai Li, Ziwei Liu, Yew Soon Ong, and Chen Change Loy. Mosaicfusion: Diffusion models as data augmenters for large vocabulary instance segmentation. *arXiv preprint arXiv:2309.13042*, 2023. 3
- [89] Zhenda Xie, Zheng Zhang, Yue Cao, Yutong Lin, Jianmin Bao, Zhuliang Yao, Qi Dai, and Han Hu. Simmim: A simple framework for masked image modeling. In *CVPR*, 2022. 3
- [90] Jiarui Xu, Sifei Liu, Arash Vahdat, Wonmin Byeon, Xiaolong Wang, and Shalini De Mello. Open-vocabulary panoptic segmentation with text-to-image diffusion models. In *CVPR*, 2023. 2, 3
- [91] Boyu Yang, Chang Liu, Bohao Li, Jianbin Jiao, and Qixiang Ye. Prototype mixture models for few-shot semantic segmentation. In *ECCV*, 2020. 3
- [92] Ruihan Yang, Prakhar Srivastava, and Stephan Mandt. Diffusion probabilistic modeling for video generation. *Entropy*, 2023. 3
- [93] Haobo Yuan, Xiangtai Li, Yibo Yang, Guangliang Cheng, Jing Zhang, Yunhai Tong, Lefei Zhang, and Dacheng Tao. Polyphonicformer: Unified query learning for depth-aware video panoptic segmentation. 2022. 3
- [94] Haobo Yuan, Xiangtai Li, Chong Zhou, Yining Li, Kai Chen, and Chen Change Loy. Open-vocabulary sam: Segment and recognize twenty-thousand classes interactively. *arXiv preprint*, 2024. 3
- [95] Elad Ben Zaken, Shauli Ravfogel, and Yoav Goldberg. Bitfit: Simple parameter-efficient fine-tuning for transformer-based masked language-models. In *ACL*, 2022. 3
- [96] Xiaohui Zeng, Arash Vahdat, Francis Williams, Zan Gojcic, Or Litany, Sanja Fidler, and Karsten Kreis. Lion: Latent point diffusion models for 3d shape generation. In *NeurIPS*, 2022. 3
- [97] Gengwei Zhang, Guoliang Kang, Yi Yang, and Yunchao Wei. Few-shot segmentation via cycle-consistent transformer. In *NeurIPS*, 2021. 9
- [98] Jian-Wei Zhang, Yifan Sun, Yi Yang, and Wei Chen. Feature-proxy transformer for few-shot segmentation. In *NeurIPS*, 2022. 3, 9
- [99] Lvmin Zhang, Anyi Rao, and Maneesh Agrawala. Adding conditional control to text-to-image diffusion models. In *ICCV*, 2023. 1, 2, 3, 7
- [100] Renrui Zhang, Zhengkai Jiang, Ziyu Guo, Shilin Yan, Junting Pan, Hao Dong, Peng Gao, and Hongsheng Li. Personalize segment anything model with one shot. In *ICLR*, 2024. 7, 8, 9
- [101] Yuxuan Zhang, Huan Ling, Jun Gao, Kangxue Yin, Jean-Francois Lafleche, Adela Barriuso, Antonio Torralba, and Sanja Fidler. Datasetgan: Efficient labeled data factory with minimal human effort. In *CVPR*, 2021. 3
- [102] Yuanhan Zhang, Kaiyang Zhou, and Ziwei Liu. What makes good examples for visual in-context learning? In *NeurIPS*, 2023. 3
- [103] Wenliang Zhao, Yongming Rao, Zuyan Liu, Benlin Liu, Jie Zhou, and Jiwen Lu. Unleashing text-to-image diffusion models for visual perception. In *ICCV*, 2023. 2, 3, 4
- [104] Chong Zhou, Xiangtai Li, Chen Change Loy, and Bo Dai. Edgesam: Prompt-in-the-loop distillation for on-device deployment of sam. *arXiv preprint arXiv:2312.06660*, 2023. 3
- [105] Linqi Zhou, Yilun Du, and Jiajun Wu. 3d shape generation and completion through point-voxel diffusion. In *ICCV*, 2021. 3

6. Appendix

Overview. In this supplementary, we present more results and details:

- **Appendix A.** More details on method.
- **Appendix B.** More empirical studies and analysis.
- **Appendix C.** More visual results and discussion.

A. More Details on Method

Implementation Details. In the training stage, we use the PNDM noise scheduler and set the whole time step as 1000. The input images are randomly resized and cropped to 256×256 . Additionally, they are flipped with a probability of 0.5. We set the time step in Ref LDM-Seg-f as 0. The AdamW optimizer use a learning rate of $1e-4$ and weight decay of $1e-2$. Our experiments are mainly conducted on 4 NVIDIA A100-80G GPUs. In the inference stage, the denoising time steps for Ref LDM-Seg-n is 20. The number of trainable parameters is 872M and 13M for the model without LoRA and with LoRA, respectively.

Derivation of Pseudo Masks. Denote the value of prediction $\tilde{P}\tilde{M}$ in position i by (x, y, z) , we get the binary mask \tilde{M} by calculating the L2 distance between $\tilde{P}\tilde{M}$ and PM_v ,

$$\begin{aligned} \tilde{M}_i \in fg \\ \iff \\ \|(x, y, z) - (b, a, \frac{a+b}{2})\|_2 > \|(x, y, z) - (a, b, \frac{a+b}{2})\|_2 \end{aligned} \quad (12)$$

It is evident that,

$$\begin{aligned} \|(x, y, z) - (b, a, \frac{a+b}{2})\|_2 > \|(x, y, z) - (a, b, \frac{a+b}{2})\|_2 \\ \iff (b-a)(y-x) > 0 \end{aligned} \quad (13)$$

As mentioned above $a < b$, we find that the results are only determined by the value in channel **0** (x) and **1** (y) of $\tilde{P}\tilde{M}$. Then we get binary mask $\tilde{M} = \tilde{P}\tilde{M}[1] > \tilde{P}\tilde{M}[0]$, where **0** and **1** mean the value in the corresponding channel.

B. More Empirical Studies

Classifier-free Guidance. Fig. 9 qualitatively demonstrates the effect of classifier-free guidance (CFG). When $\gamma_q = 1$ and $\gamma_\tau = 1$, the denoising process degenerates into a trivial form, resulting in more missing or false-positive predictions. Moreover, the in-context instructions are essential in our model (the third and fourth columns). Ref LDM-Seg-n fails to segment the target regions accurately with weak visual guidance.

Comparison with SegGPT. Tab. 6 compares our Ref LDM-Seg-f with SegGPT [83] on PASCAL and COCO dataset.

Table 6. Comparison with SegGPT on PASCAL and COCO dataset.

Method	PASCAL		COCO	
	mIoU	FB-IoU	mIoU	FB-IoU
SegGPT [83]	80.3	91.6	50.8	77.0
Ref LDM-Seg-f (ours)	83.4	92.0	59.6	82.7

C. More Visual Results

Denoising Process of Ref LDM-Seg-n. Fig. 8 provides more examples to demonstrate how Ref LDM-Seg-n generates pseudo masks in the inference stage. Starting from Gaussian noise, Ref LDM-Seg-n gradually denoises and differentiates the foreground and background regions. The outputs align with the augmented pseudo masks PM_a (the sixth column). It is evident that the information of query images is fused into the segmentation mask.

More Visualization on images and videos. Fig. 11 and Fig. 12 provide more visual results on COCO and VSPW. Our model performs well across different scenarios and categories.

Failure Cases Analysis. We show some failure cases in Fig. 10. These samples exhibit significant changes in attitude, focus, or size from the prompts to the queries. Our model fails in these hard examples.

Limitations and Future Work. According to previous works [64, 66], huge amounts of training data are essential to exploit the potential of LDM fully. To this end, we will scale up the training data in our future work. We also consider scaling up the parameters if more training data is available. Moreover, we will explore more advanced prompt encoder architectures and prompt engineering methods.

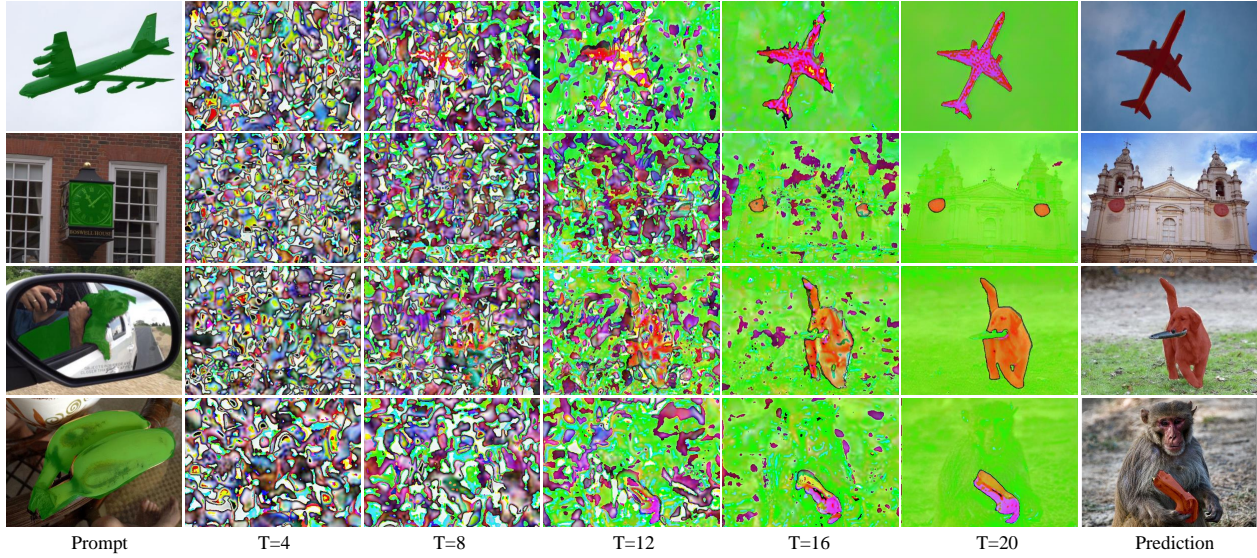


Figure 8. More visual results of Ref LDM-Seg-n at different time steps.

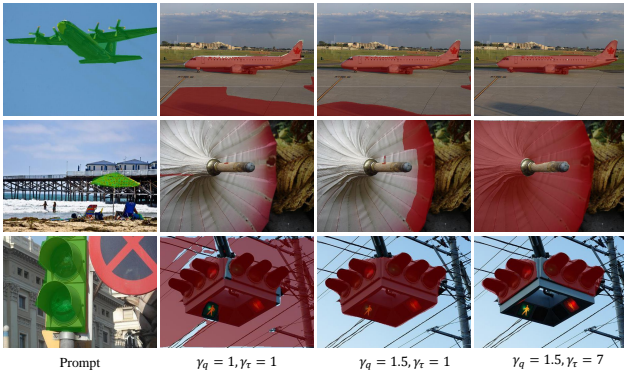


Figure 9. Effect of classifier-free guidance. The prompt and segmentation results are labeled in green and red, respectively.

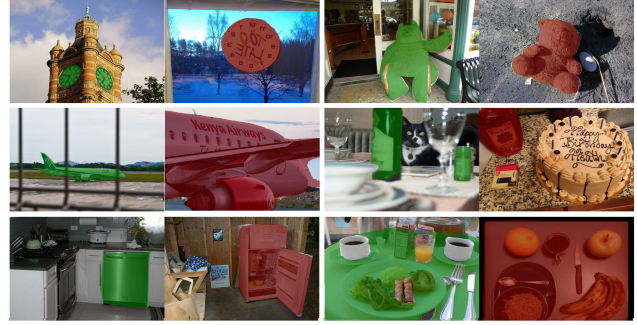


Figure 11. More visual results of Ref LDM-Seg-f on COCO dataset.



Figure 10. Failure cases of COCO dataset. **Left:** Visual prompts. **Right:** Segmentation results.

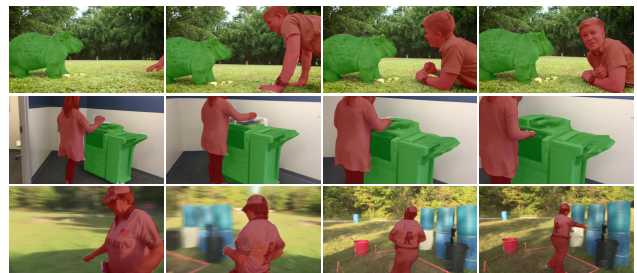


Figure 12. More visual results of Ref LDM-Seg-f on VSPW dataset.